1 Influence of Wind on Isotherm Tilt

1.1 Introduction

In 2000, King County Department of Natural Resources and Parks (KCDNRP) implemented a five-year program to develop a set of computer models to understand how the growing human population and associated land use changes would affect Lakes Washington and Sammamish. As part of this program, an extensive field monitoring program was developed for Lake Washington. The resulting data provided a rich source of information for studying relations between the lake hydrodynamics and the phytoplankton (diatoms) population. Such an understanding is important when assessing how human effects propagate into physical and/or biological changes in Lake Washington.

In the 2003 and 2004 KCDNRP field studies, diatom biovolume concentration was observed to differ along the length of the lake. The central part of the lake had higher concentrations (Figure 1. 1), and early-spring temperature profiles showed a persistent north-to-south tilt of the isotherms (Figure 1. 2).

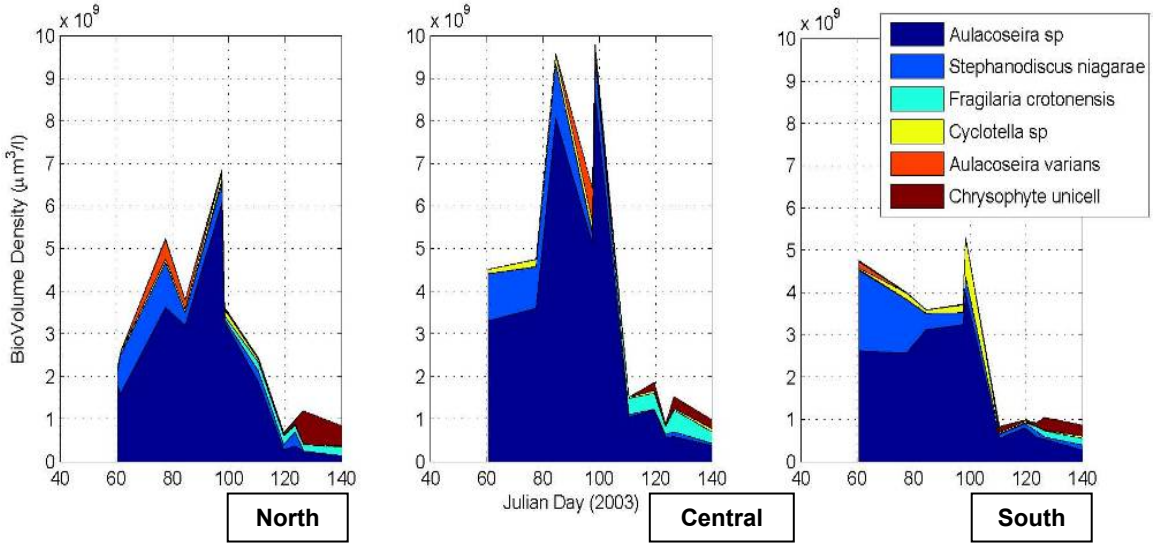

Figure 1. 1. Most abundant species that comprised the phytoplankton population for year 2003.

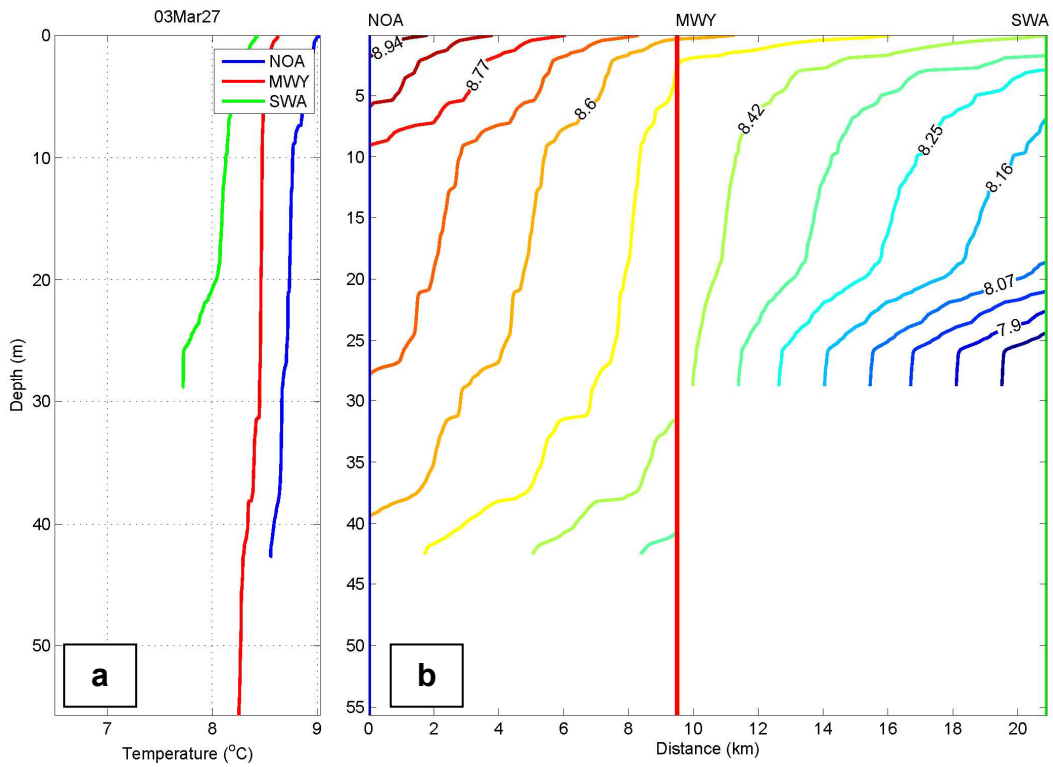

Figure 1. 2. Temperature profiles (a) and isotherm contours (b) taken March 27, 2003 (JD 85.5) at the NOA (blue), MWY (red), and SWA (green). For the isotherm contours, station locations are noted by the colored vertical lines.

Very few Lake Washington studies have investigated the physical (longitudinal) structure of the lake prior to and during the spring diatom bloom. As a result, we have an incomplete picture of how hydrodynamics affect phytoplankton dynamics along the longitudinal direction. Because phytoplankton have evolved to exist in the pelagic environment (Reynolds, 1984), a better understanding of the physics that control the pelagic environment would seem useful for a better understanding of phytoplankton dynamics.

1.1.1 Previous Studies in Lake Washington

Lake Washington is located in a very urbanized area within greater Seattle WA, a metropolitan area of some 1.5 million people surrounding the lake (Figure 1. 3). The lake is the second of three lakes in a chain. Lake Sammamish is the first of the chain and drains into the Sammamish River, which flows into the north end of Lake Washington. Just north of the center of Lake Washington, the lake drains into a third lake, Lake Union. Lake Washington is approximately 33 kilometers in length and 2.5 kilometers in width; the length is orientated in a north-south direction. The lake has a

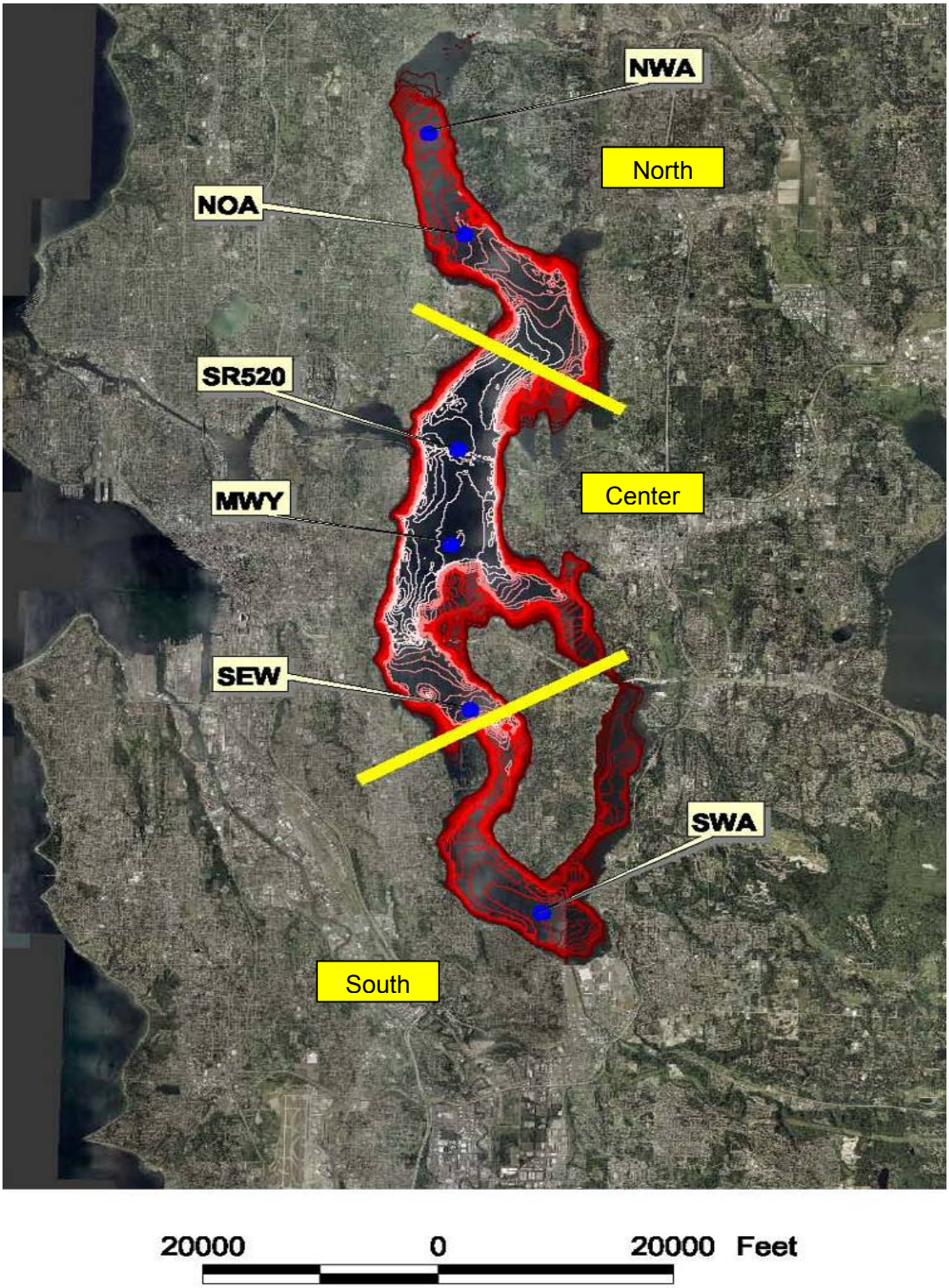

Figure 1. 3. Lake Washington study area and field stations NWA, NOA, SR520, MWY, SEW, and SWA. Bathymetric contours are shown to present bottom relief and North is aligned with the page. Yellow lines demark the three general regions of the lake: north, center, and south.

surface area of approximately 84 km^2 and an average depth of approximately 35 meters; the greatest depth is approximately 70 meters near the center of the I90 Bridge. Lake Washington's two primary water sources are the Cedar River at the south end and the Sammamish River at the north end. The Cedar contributes about 57% and the Sammamish about 27% of the annual inflow; the other 16 % is from tributary streams and rainfall. The hydraulic residence time is approximately 2.4 years. The temperate climate of the region makes Lake Washington a monomictic lake.

Lake Washington has been studied and written about most for its rapid recovery from sewage discharges that were diverted from the lake in the late 1960s. This story is best summarized by Edmondson (1994). Because the emphasis was on the recovery of the entire lake, analyses focused on the lake as a whole and typically sampled at a single location (Edmondson, 1972; Richey, Devol, and Perkins, 1975; Lehman, 1978; Devol and Packard, 1978; Richey, 1979; Edmondson and Lehman, 1981).

The lake's seasonal succession of phytoplankton was indirectly described by Edmondson and Litt (1982) and Infante and Edmondson (1985) in their analyses of zooplankton dynamics. During July, longitudinal zooplankton distributions were considered insignificant, but phytoplankton distributions were not assessed (Edmondson, 1985). The under-studied seasonal succession was noted by Arhonditsis, Brett, and Frodge (2003), who analyzed environmental conditions that controlled the timing and spatial development of the bloom. Lake physics, however, was represented by water temperature, which produced inconclusive results. Spatial variability was considered substantial but small compared to temporal variability, but the lake could be divided into three areas: northern, central, and southern. Generally, *Chlorophyll a* and inorganic phosphorous (limiting nutrient) were higher at the north end of the lake compared to the south end. The north/south difference was ascribed to nutrient loads from the Cedar and Samammish Rivers; the Samammish has higher nutrient loads compared to the Cedar.

The seasonal character of the phytoplankton can be divided into four modes, which were determined from an integrated data set that represented the whole lake

(Arhonditsis, Winder, Brett, and Schindler, 2004). Incident solar radiation was found to control phytoplankton growth from January to March, and total phosphorous and caldoceran abundance was found to control phytoplankton growth from April to June. The initiation of the spring bloom was found to precede thermal stratification of the water column (Arhonditsis, Winder, Brett, and Schindler, 2004). Typically, the spring bloom was thought to occur when stratification limited vertical mixing such that the depth-integrated production exceeds losses (Sverdrup, 1953). The pre-stratification bloom spawned one of the few discussions on how physics (hydrodynamics) can control the phytoplankton bloom in Lake Washington. The argument was that the bloom occurred when vertical mixing (eddy diffusion) relaxed sufficiently so that the net growth rate exceeded downward vertical fluxes (diffusive flux). They suggested this condition would occur during a period of calm winds or temporary warming of the surface layer. This dynamic balance between growth and vertical diffusion was discussed by Sverdrup (1953) and theoretically developed by Huisman et al. (1999).

For Lake Washington, Walters (1980) developed a coupled thermal and biological model and investigated relations between vertical turbulent transport of thermal energy and nutrient and phytoplankton response. Prior to the spring bloom, he found phytoplankton production was small because of the large mixing depth, but there were times when incident solar radiation was sufficient to promote growth (Walters, 1980). Phytoplankton was diffused out of the photic zone faster than it could grow, but there was sufficient light if the phytoplankton could stay in the photic zone longer. This condition was suggested by Arhonditsis, Winder, Brett, and Schindler (2004). In the Walters (1980) model, the phytoplankton bloom occurred when vertical mixing was suppressed by increased temperatures (initiation of thermal stratification). From January to February, Syck (1964) found differential cooling was an important process in transporting surface water to the lake bottom. However, when stratification was more pronounced during the spring, bottom mixing was controlled by wind when spring storms mixed surface water to the bottom (Syck, 1964).

The Lake Washington spring phytoplankton bloom is dominated by diatoms; *Aulacoseira subarctica* is typically the most abundant diatom (Infante and Edmondson, 1985; Edmondson, 1997; Arhonditsis, Brett, and Frodge, 2003). During the spring, *Aulacoseira sp.* is the most frequently consumed diatom by the

zooplankton population, and during the winter *Diaptomus (Leptodiaptomus) ashlandi* and *Daphnia pulicaria* are maintained by *Aulacoseira italica* and *Stephanodiscus astrea* (Infante and Edmondson, 1985). But the peak *D. (L.) ashlandi* population occurs before the peak *D. pulicaria* population, and *D. (L.) ashlandi* numbers and clearance rates can be sufficient to control the early spring diatom population (Edmondson and Litt, 1982). *Aulacoseira* and *D. (L.) ashlandi* play an important role in the dynamics of the spring bloom.

From about March 15 to March 29 of 2001, *Cyclops bicuspidatus* densities were greater at the north end of the lake than at the south end. Some of the north/south variation was due to grazing pressure by emigrating sockeye salmon fry from the Cedar River, but this grazing affected between 5% and 12% of the zooplankton biomass (Beauchamp et al., 2004). *D. pulicaria* and *D. (L.) ashlandi* were sampled, but north/south differences were not mentioned. The March time interval preceded the spring diatom bloom, which peaked near the end of March for years 2003 and 2004 (presented in Section Two). Adult copepods that are carnivorous may be more herbivorous during earlier stages in their life (Brandl, 2005; Moore, 1979). Moore (1979) found *C. bicuspidatus* diet varied with its developmental stage: stage nauplii (N)-III to N-V diet contained mostly detritus and some phytoplankton; stages copepod (C)-I to C-III contained detritus and a larger portion of phytoplankton; and stages C-IV to C-VI contained rotifers, nauplii, copepods (some *D. (L.) ashlandi*), and cladocerans.

1.1.2 Other Lake Studies

The physical structure of the lake affects the amount of light, nutrients, and temperature that phytoplankton may experience in the water column. Temperature and light are important environmental variables that affect phytoplankton growth and species succession (Foy and Gibson, 1993; Sebastian, Interlandi, and Kilham, 2001; Arhonditsis, Winder, Brett, and Schindler, 2004; Sommer, 1994), and differences in these variables cause spatial and temporal differences in species composition and density (Felip and Catalin, 2000; Barbiero et al., 2000). Changes in vertical mixing depth can be an important dimension in determining species compositions (Wall, Briand, and Ottawa, 1980; Viner and Kemp, 1983). For almost all lakes, the horizontal scales are orders of magnitude larger than the depth. The horizontal

patchiness of phytoplankton is a function of the horizontal scale considered. In general, horizontal mixing smears plankton patches at scales greater than one kilometer and creates fairly uniform concentrations at scales less than one kilometer. At scales greater than one kilometer, phytoplankton growth rates exceed the effective rate of horizontal diffusion, so phytoplankton patchiness is more likely at scales greater than one kilometer (Harris, 1980; Zavoruyev et al., 1992). The patchiness depends on the relative growth rate (typically one division per day) and the horizontal eddy diffusion rate (Harris, 1980). Because Lake Washington is 33 km long, spatial differences would be determined by biological growth rates when hydrodynamic transport time scales (by eddies or velocity) are longer than biological growth time scales.

Spatially variable hydrodynamic conditions are known to create spatially variable phytoplankton populations. However, the supporting studies preferentially investigate stratified systems. Stratification limits nutrient fluxes into nutrient-depleted areas of the water column; nutrient fluxes limit phytoplankton growth (Eckert, Imberger, and Saggio, 2002; Robarts et al.,1998; Saggio and Imberger, 2001; MacIntyre et al., 1999; MacIntyre and Jellison, 2001; Sharples et al., 2001). These studies investigated the relations between internal-waves and vertical mixing near physical boundaries and associated nutrients fluxes into the depleted areas; internal wave energy is converted to mixing (MacIntyre et al., 1999; MacIntyre and Jellison, 2001; Stevens et al., 2005; Saggio and Imberger, 1998, Eckert, Imberger, and Saggio, 2002). Where nutrient availability is not as limited, overturning eddies can expose phytoplankton to different light intensities; the photosynthesis rate will change if the photo-adaptive time scale is less than the overturning time scale (MacIntyre, 1998).

Tilted isotherms will produce a spatially variable mixed layer depth along the tilt. The mixed layer depth affects phytoplankton growth rate through the depth-averaged photosynthesis rate; a longitudinally varying mixed layer depth creates a longitudinally varying growth rate. In Lake Superior, up-tilting of the thermocline produced a significant response in the *Chlorophyll a* biomass inhabiting the metalimnion (Zhou et al., 2001). The up-titling increased the available light in the metalimnion and the event had sufficient duration that the phytoplankton could respond to the increased light. In Kootenay Lake in British Columbia, Canada, a

persistent longitudinal tilt was observed in the isotherms with the downwind end being completely mixed over the depth. This condition resulted from wind events that had a shorter period compared to the period of the internal seiche (Stevens et al., 1996; Wiegand and Carmack, 1986). Because the lake is so long (100 km), the internal seiche period is much larger than the period of the wind events, which can modify the internal seiche before it has cycled through the lake (Wiegand and Carmack, 1986). Relative to the period of the internal seiche, short wind event periods can modify the internal seiche and maintain a tilted isotherm.

The magnitude of the tilt is dependent on the length of the lake, stratification, and the surface wind stress (Spigel and Imberger, 1980; Stevens and Gregory, 1997; Monismith 1986: Stevens and Imberger, 1996). Tilting will be more dramatic during the spring when density differences are small and small barotropic tilts can create large baroclinic responses. When the isotherms surface at the upwind end of the lake, upwelling is significant and bottom water is advected to the surface. Concurrently at the down wind end of the lake, down welling and vertical mixing create a well-mixed region deeper than the thermocline (Stevens and Imberger, 1996; Farrow and Stevens, 2003; Verhagen, 1994; Monismith 1986). For a tilt that persists longer than the phytoplankton time scale, a longitudinal tilt in the thermal structure will produce a longitudinally varying phytoplankton biomass.

1.1.3 Study Goals and Hypothesis

The study's goal is to determine the level of importance that hydrodynamics have in defining the spring diatom bloom in Lake Washington, from timing and size of the bloom to longitudinal distributions of phytoplankton concentrations. Two studies suggested the relaxation of vertical eddy diffusion is important in allowing the bloom to develop (Walter, 1980; Arthonditsis, Winder, Brett, and Schindler, 2004). No previous Lake Washington study has concurrently investigated the relative effects of nutrients and hydrodynamics on the spring diatom bloom, as does this study.

The hypothesis is that the hydrodynamics that determine the observed isotherm tilt also cause the longitudinal phytoplankton differences observed between the northern, central, and southern areas of the lake. The tilted isotherms create a

longitudinally varying mixed layer depth, which affects the depth-integrated photosynthesis rate.

In Section One I show how wind stress is the dominant force that maintains the isotherm tilt. I present the governing equations between surface wind stress and horizontal density gradient and relate these equations to the Wedderburn Number (W_N). W_N is a non-dimensional number that describes the balance between surface wind stress and horizontal density gradients.

In Section Two I show how the isotherm tilt affects the depth-integrated photosynthesis rate. I develop a simple one-dimensional Advection-Diffusion model relating vertical mixing and phytoplankton growth kinetics. I use the model to show how the isotherm tilt decreases the depth-integrated photosynthesis rate at the north end, and how upwelling and horizontal advection associated with the tilt dilute and transport phytoplankton out of the south end. I also show that the diatom bloom occurred when vertical eddy diffusion relaxed by a factor of sixty.

1.2 Methods

1.2.1 Field Monitoring Program

The Lake Washington field monitoring program was performed by KCDNRP for years 2003 and 2004. The primary objective was to characterize the thermal and hydrodynamic evolution of the lake along the longitudinal direction, with additional objectives to collect hydrographic information for a hydrodynamic computer model and assess effects from the floating bridges. The 2004 field monitoring was specifically designed to monitor conditions during the spring diatom bloom.

The field monitoring program must start before the bloom and continue until the bloom is over; the spring diatom bloom typically starts in mid-March and ends by mid-June (Arhonditsis, Brett, and Frodge, 2003). To capture the spatial dynamics of the isotherm tilt and phytoplankton, field stations must be located in the longitudinal direction of the lake. The tilt results from internal waves that are set up by the wind stress; the wave's modal structure can be determined from a single point at the center of the lake along the longitudinal direction. A centrally located station can capture the dynamics of the internal waves. Stations located north and south of the

center will add detail to the internal wave dynamics and provide information on upwelling and down welling. Three longitudinally spaced phytoplankton field stations are required to assess spatial dynamics; stations will be co-located with hydrodynamic field stations (see Section Two for a detailed description).

1.2.1.1 Field Instruments

The field objectives required measuring flow and temperature over time. Three types of instruments were used: Richard Brancker Research (RBR) XR-420 T24 thermistor arrays that measured temperature; Precision Measurement Engineering Self-Contained Autonomous MicroProfiler (SCAMP) that measured temperature micro-structure and fluorescence; and Sontek 1500 kHz Acoustic Doppler Profilers (ADP) and RD Instrument 300 kHz Workhorse Acoustic Doppler Current Profilers (ADCP) that measured velocity. The RBRs and dopplers provide a time history of events while the SCAMP provided a synoptic view over space.

The SCAMP was configured with a Li_Cor LT-192SA Photosynthetically Active Radiation sensor, a Fluorometer sensor with a 455 nanometer excitation diode, and two channels for fast temperature and temperature-gradient response; each channel was equipped with a FP07 glass thermistor manufactured by Thermometrics, Inc. The FP07 thermistors have an operating range between 0 ^{o}C and 30 ^{o}C with an accuracy of 0.05 ^{o}C and a resolution of 0.001 ^{o}C. The SCAMP was calibrated for descent rate of about10 (cm/sec). The SCAMP was factory calibrated before each year's study.

The RBR thermistor arrays had 24 thermistors spaced at one-meter intervals. The thermistors have an operating range between -5 ^{o}C to 35 ^{o}C and an accuracy of ±0.005 ^{o}C. Each RBR thermistor was equipped with an RBR DR-1050 depth sensor, which records water depth every hour. The data loggers were programmed for a three-minute sample interval, which was near the thermal response time of the thermistors.

The Sontek and RDI were programmed for autonomous operation with a sampling interval of 45 minutes. Measurement accuracy is a function of the number of samples (ensemble) averaged per recorded value; ensemble sizes were selected for

a maximum velocity error of 0.5 cm/sec for the Sontek and 0.8 cm/sec for the RDI. The RDI was programmed to sample every two meters of the water column and the Sontek was programmed to sample every one meter of the water column. The sampling interval, ensemble size, and sample depth interval were selected to optimize battery life (approximately 40 days) and data collection.

1.2.1.2 Field Monitoring Program

Five field stations were selected along the length of the lake for SCAMP profiles. These stations were North Washington (NWA), north of the NOA facility at Sand Point (NOA), mid-way between the SR520 and I-90 bridges (MWY), north of Seward Park (SEW), and South Washington (SWA); see Figure 1. 3. The five stations were selected for their geographical features: NWA, NOA and SWA represented the shallow ends of the lake; MWY represented the deepest central part; and north of Seward Park (SEW) where the bathymetry showed a steep change in water depth. Water depths at the stations are given in Table 1. 1 and bathymetric contours are illustrated in Figure 1. 3. SCAMP profiles were taken from a boat.

Table 1. 1 Water depths at each monitoring location.

Station	Depth (m)
NWA	32
NOA	42
SR520	62
MWY	58
SEW	47
SWA	31

For the year 2003 starting in March, the SCAMP field plan required weekly profiles until mid-June; however, weather, instrument reliability, and staff availability allowed only three profiles during the March to May period. For the year 2004 starting in March, the SCAMP field plan required weekly profiles until the profiled fluorescence approximately doubled from the first profile, whereupon profiles were increased to twice per week. Weather interfered, however, with the twice-weekly rate and SCAMP profiles stopped after the April 16 field run because the instrument broke down.

For the year 2003, three RBRs were deployed at SR520 Bridge and one RBR was located at SWA. Three arrays were located at the SR520 location, one array was

located on the bridge (SR520C) and two others were placed north of the bridge at about 200-meter increments (SR520N1 and SR520N2; SR520N2 was the northern most array). In year 2004, three RBRs were deployed, one each at NOA, MWY, and SWA. The devices were moored so the array was approximately 3-5 meters below the water surface (Table 1. 2); this design considered instrument safety to reduce the chance that a deep draft boat would strike the instruments.

Table 1. 2. RBR thermistor array operating depth ranges (meters) at the associated field stations.

Station	Year 2003 (m)	Year 2004 (m)
SR520C	2 - 25	NA
SR520N1	16 - 40	NA
SWA	5 – 28	5 – 28
MWY	NA	5 – 28
NOA	NA	3 – 26

For years 2003 and 2004, the RDI was moored on the lake bed at MWY and the Sontek was attached to the SR520 floating bridge and pointed downward.

All data was subject to a visual inspection for quality assurance. The SCAMP and doppler data had no obvious errors. During the 2003 RBR field program, water leaked into the thermistor housing and caused significant thermistor drift or complete failure; the SR520N2 completely failed and the SR520N1 and SWA showed drift in some of the thermistors. Of the 24 thermistor channels, 4 were corrupt in the SWA unit, 3 were bad in the SR520N1 unit, and the SR520C unit was fine; the bad channels were deleted for the analysis (Figure 1. 4). The 2004 RBR thermistors had no obvious errors; the units had been repaired by the manufacturer.

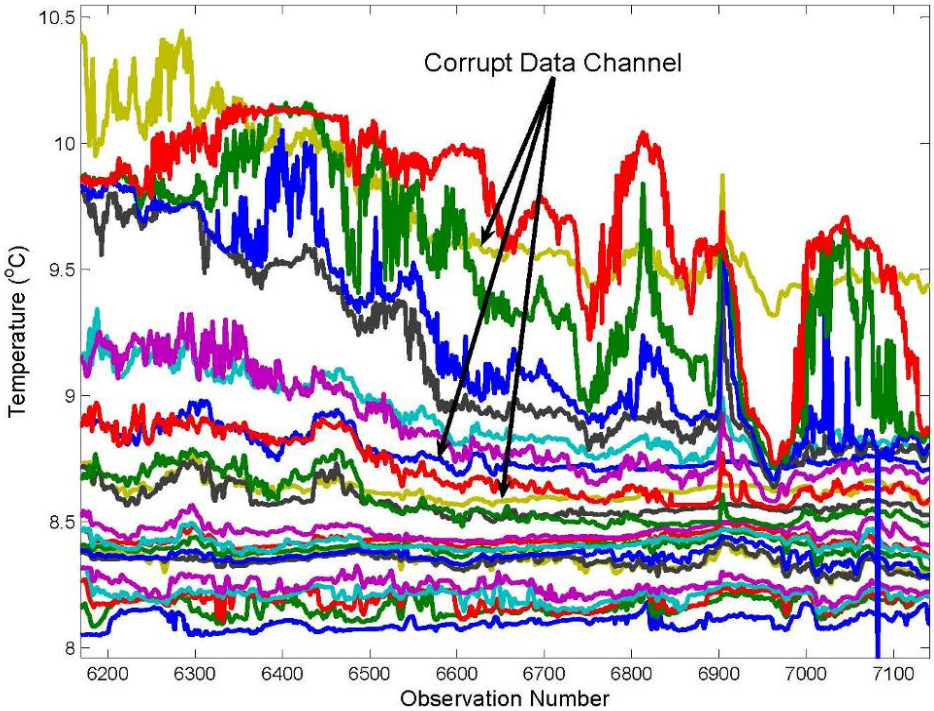

Figure 1. 4. Identification of three of the four corrupted temperature channels in the RBR thermistor located at SWA; temperature readings drifted across neighboring temperature readings. Each line is a thermistor at a set depth.

1.2.2 Atmospheric Observations

Because the isotherm tilt is hypothesized to result from surface wind stress, and because the thermal structure of the lake depends on heat transfer into and out of the lake (Fischer et al., 1979), atmospheric data are required concurrent to the hydrodynamic field monitoring program.

Wind speed and direction and air temperature were obtained from the atmospheric station on the I-90 floating bridge; the station, located at the middle of the bridge, is maintained by the Washington Department of Transportation (WADOT). The anemometer was located about 12 meters above the water surface and winds were adjusted to a 10-meter height above the water for computing wind stress at the water surface; wind speed was adjusted using a power-law relation by Hsu et al. (1994). Observations were recorded at 15-second intervals and were integrated into one-hour averages. For both years, the winds were predominantly from the south (Figure 1. 5 and Figure 1. 6). In year 2004 winds were a little more spread in direction and

had higher velocities than in 2003. In 2003, the southward wind occurred between April 24 and April 29.

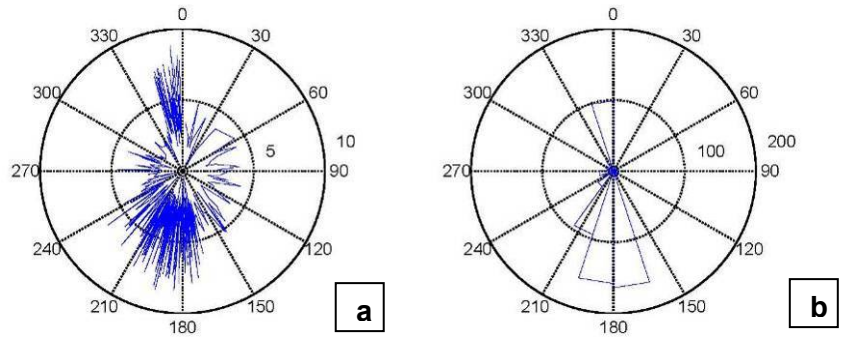

Figure 1. 5. Wind roses for the April 2003 period of study. Wind direction and magnitude (a) where north is 0° and east is 90°, wind direction is from the noted degree, and magnitude is denoted by the radial grid, maximum grid is 10 m/s. Directional frequency (b) is denoted by the radial grid, maximum grid is 200 counts. The strong southward winds occurred from April 24th to 29th.

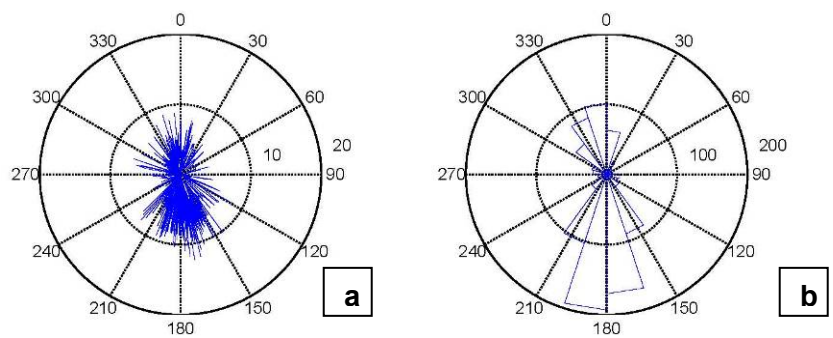

Figure 1. 6. Wind roses for the March 2004 period of study. Wind direction and magnitude (a) where north is 0° and east is 90°, wind direction is from the noted degree, and magnitude is denoted by the radial grid, maximum grid is 20 m/s. Directional frequency (b) is denoted by the radial grid, maximum grid is 200 counts.

Solar radiation, atmospheric pressure, and relative humidity were obtained from the University of Washington (UW) Atmospheric Sciences building on the UW campus. The building is located approximately 2.3 miles west of the SR520 field station. Measurements were recorded at one-minute intervals and integrated into one-hour averages. In 2003 the average solar radiation was about 190 (W/m^2) and in 2004 it was about 280 (W/m^2). Average air temperature was about 10 ^oC in 2003 and about 14 ^oC in 2004 (Figure 1. 7). Year 2004 had stronger winds, higher solar radiation and air temperatures compared to year 2003. Date conversions between Julian Day (JD) and the Gregorian calendar are given in Table 1. 3.

In 2004 parts of I-90 Bridge weather data was missing. The missing intervals were generated from weather observations at the University of Washington Atmospheric Sciences Building. Relations were generated using simple regression models. Wind speed and air temperature were synthesized for JD 86 to 88.5 and JD 95 to 99. Wind direction was not estimated because vector regressions were unsatisfactory.

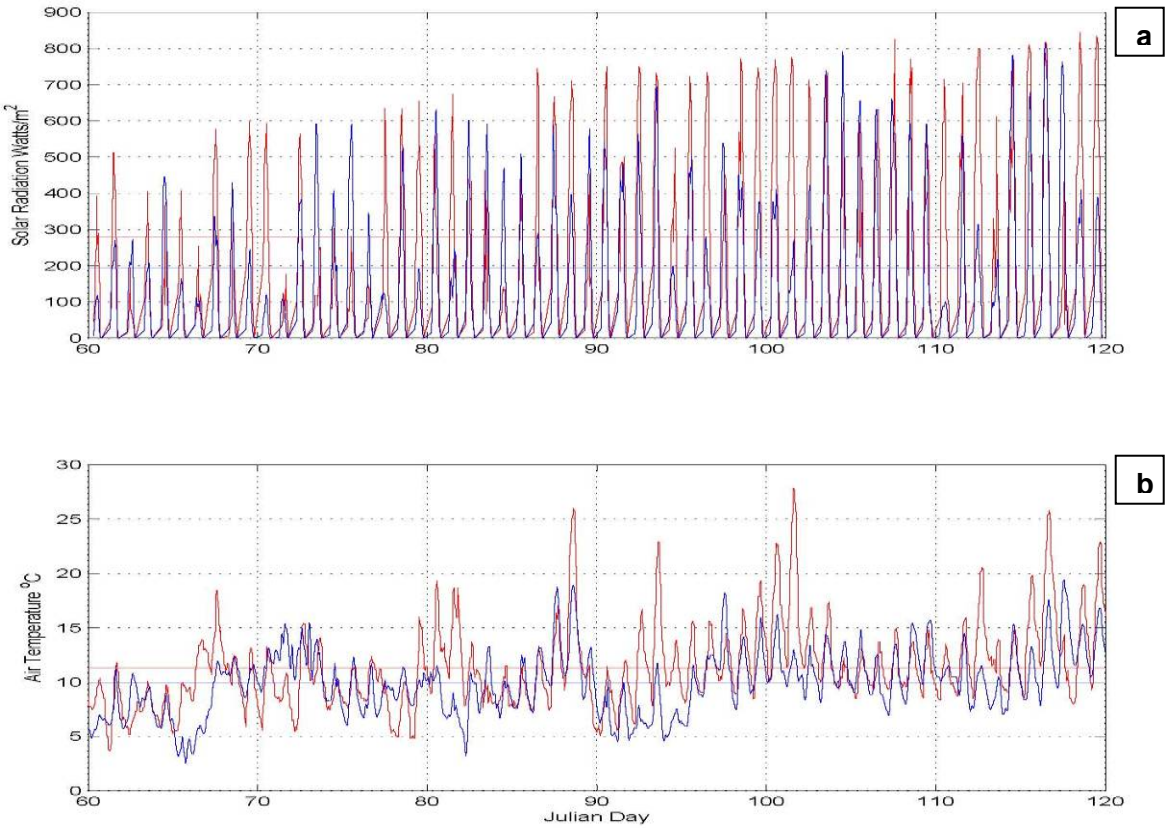

Figure 1. 7. Observed solar radiation (a) and air temperatures (b) for years 2003 (blue) and 2004 (red). The straight lines are the average condition over the given period; year 2004 is red and year 2003 is blue. In 2004, solar radiation and air temperature was higher compared to the same period in 2003.

Table 1. 3. Conversion between Julian Day and Gregorian Calendar.

Julian Day	2003	2004
60	March 2	March 1
120	May 1	April 30

1.2.3 Analytical Methods

To investigate the hypothesis that the surface wind stress maintains the observed isotherm tilt, one must develop a physical relation between the surface wind stress

and the isotherm tilt. The isotherm tilt is a baroclinic pressure gradient along the horizontal direction (longitudinal direction for Lake Washington). The balance between the surface wind stress and the baroclinic pressure gradient is represented in the Wedderburn Number, which is a non-dimensional scaling number that represents a steady-state balance between the baroclinic pressure force and the surface stress (Spigel and Imberger, 1980; Imberger and Patterson, 1990). This balance is derived from the horizontal momentum equation.

1.2.3.1 The Balance between Surface Wind Stress and the Baroclinic Pressure Gradient

The balance between surface wind stress and the baroclinic pressure gradient is most easily studied for a simple two-layer system (Figure 1. 8). The linear momentum equations for a two-layer system are given by (1.1) (non-linear effects are discussed later).

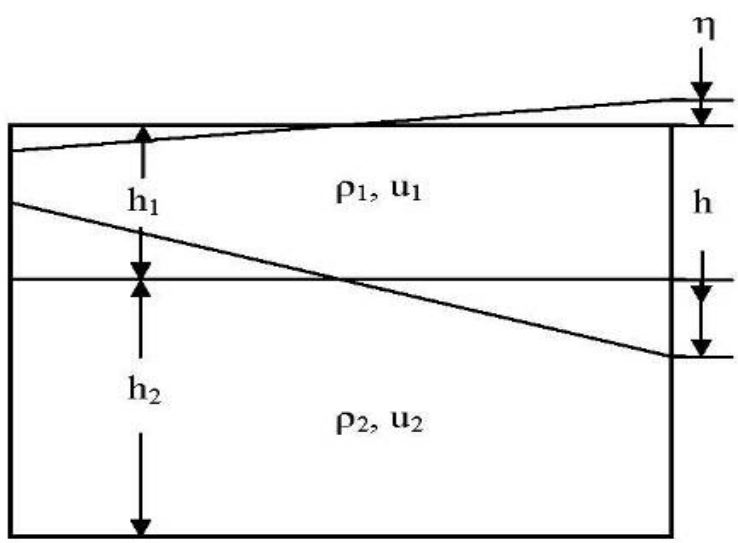

Figure 1. 8. Schematic of a simple two-layer system comprised of the surface layer of depth h_1, density ρ_1, and velocity u_1 and the bottom layer of depth h_2, density ρ_2, and velocity u_2.

$$\frac{\partial u_1}{\partial t} = -g\frac{\partial \eta}{\partial x} + \nu\frac{\partial^2 u_1}{\partial z^2}$$
$$\frac{\partial u_2}{\partial t} = -g\frac{\rho_1}{\rho_2}\frac{\partial \eta}{\partial x} - g\left(1-\frac{\rho_1}{\rho_2}\right)\frac{\partial h}{\partial x} + \nu\frac{\partial^2 u_2}{\partial z^2} \qquad (1.1)$$

Where u_1 is the upper and u_2 is the lower horizontal velocity, ρ_1 is the upper and ρ_2 is the lower density, η is the upper and h is the lower interface displacement, v is

kinematic viscosity (Figure 1. 8). Integrating (1.1) over each layer depth and subtracting the two equations gives (1.2).

$$\frac{\partial U_{12}}{\partial t} = g\left(\frac{\rho_1}{\rho_2} - 1\right)\frac{\partial \eta}{\partial x} + g\left(1 - \frac{\rho_1}{\rho_2}\right)\frac{\partial h}{\partial x} + \frac{u_*^2}{B_1} - \left(\frac{H}{B_1 B_2}\right)\nu \left.\frac{\partial u}{\partial z}\right|_{\text{interface}} + \frac{C_B u_B^2}{B_2}$$

$$\frac{\partial U_{12}}{\partial t} = \frac{\partial U_1}{\partial t} - \frac{\partial U_2}{\partial t} \tag{1.2}$$

$$B_1 = \eta + h_1 - h$$

$$B_2 = h_2 + h$$

$$u_*^2 = \nu \left.\frac{\partial u}{\partial z}\right|_{\text{surface}} = U_{10}^2 \frac{\rho_{air}}{\rho_{water}} C_D$$

$$u_B^2 C_B = \nu \left.\frac{\partial u}{\partial z}\right|_{\text{bottom}} \tag{1.3}$$

Where U_1 and U_2 are the depth average horizontal velocity, h_1 and h_2 are the upper and lower layer thickness, H is the total depth, u_* is the surface friction velocity, U_{10} is the wind speed 10 meters above the water surface, ρ_{air} is the air density, ρ_{water} is the surface water density, C_D is the surface drag coefficient, C_B is the bottom drag coefficient, and u_B is the bottom velocity.

The upper interface displacement η is typically orders of magnitude smaller than the lower interface displacement h, $\eta \approx h(1-\rho_1/\rho_2)$ and the surface wave (η) travels orders of magnitude faster than the interfacial wave (h) (Gill, 1982). Because the surface wave travels away from the interfacial wave so rapidly, the interfacial wave can be studied separately by letting $\partial\eta/\partial x \approx 0$; η is important in defining the initial displacement of h but can be ignored when studying the resultant dynamics of h. Rewriting (1.2) for $\partial\eta/\partial x \approx 0$ gives (1.4).

$$\frac{\partial U_{12}}{\partial t} = g\left(1 - \frac{\rho_1}{\rho_2}\right)\frac{\partial h}{\partial x} + \frac{u_*^2}{B_1} - \left(\frac{H}{B_1 B_2}\right)\nu \left.\frac{\partial u}{\partial z}\right|_{\text{interface}} + \frac{C_D u_B^2}{B_2} \tag{1.4}$$

In (1.4), the left-hand side is the acceleration of the baroclinic mode of the two-layer system. On the right-hand side, the first term is the density-adjusted pressure gradient, the second term is surface wind stress, the third term is the shear stress at the interface, and the fourth term is the bottom stress. The velocity shear and

bottom velocity were estimated from the observed velocity profiles at MWY and the friction velocity was estimated from the observed wind speeds for year 2003. The wind stress was 10^2 times larger than the bottom stress and 10^5 larger than the interface shear stress (Table 1. 4); therefore, (1.4) can be simplified by eliminating the interface and bottom stress terms (1.5).

Table 1. 4 Mean value of the three stress terms (u_*^2, u_B^2, and $\partial u/\partial z$) calculated from observed wind and water velocities from the March 2003 observations. Statistics for the velocity shear are based on the absolute value of the observations.

Stress Term	Mean	Standard Deviation	Coefficient	Mean Stress (m^2/sec^2)
u_*^2 (m^2/sec^2)	5.3×10^{-4}	9.93×10^{-4}	$C_D\approx1\times10^{-3}$ (unit less)(1)	5.3×10^{-4}
u_B^2 (m^2/sec^2)	2.8×10^{-3}	3.46×10^{-3}	$C_B\approx2\times10^{-3}$ (unit less)(2)	5.6×10^{-6}
$\partial u/\partial z$ (1/sec)	2.9×10^{-3}	2.3×10^{-3}	$\nu\approx1.\ 3\times10^{-6}$ (m^2/sec)	3.7×10^{-9}

1. Stevens and Lawrence (1997).
2. Johnson, Kim, and Nail (2003).

$$\frac{\partial U_{12}}{\partial t} = g\left(1-\frac{\rho_1}{\rho_2}\right)\frac{\partial h}{\partial x} + \frac{u_*^2}{B_1} \qquad (1.5)$$

The acceleration is determined by the reduced gravity (baroclinic) pressure gradient and the surface wind stress (1.5). Starting from a quiescent state and imposing a wind stress ($\partial h/\partial x=0$ and $u_*^2>0$), acceleration is dominated by the wind stress until the baroclinic pressure gradient develops sufficiently to oppose the wind stress, which develops in about one-quarter of the seiche period (T/4) (Imberger, 1985). At time T/4, the tilt is in equilibrium but the internal seiche will over-shoot the equilibrium position and oscillate about the equilibrium position until time T/2 (Spigel and Imberger, 1980). The seiche period is determined by (1.6) for a two-layer system (Turner,1973).

$$T_n = \frac{2L}{n}\left(g'\frac{h_1 h_2}{h_1+h_2}\right)^{-1/2} \qquad (1.6)$$

Where n is number of nodal points in the horizontal and T_n is the associated period; for the first mode seiche n is equal to one and $T=T_1$.

When the wind stress stops ($\partial h/\partial x>0$ and $u_*^2=0$), the baroclinic pressure gradient determines the acceleration and the interface (seiche) oscillates freely with period T for small amplitude waves ($h<<h_1$). If the wind does not stop but relaxes to a lesser value, the interface tilt will relax to a lesser tilt but the relaxation time will be greater

than the time required for a freely oscillating seiche. The relaxation time is greater because the acceleration is reduced by the wind stress ($\partial h/\partial x > u_*^2$ but $u_*^2 > 0$). If the wind stress was periodic but always greater than zero, the greater relaxation time would allow more time between large events compared to a periodic series that goes to zero. Because the wind stress never goes to zero, the time average wind stress is greater than zero and a tilt will always be present; the baroclinic term must balance the imposed wind stress.

The pressure gradient and wind stress can be simplified by scaling $\partial h \approx h_1$, $\partial x \approx L$, and assuming an average surface wind stress over the lake for average conditions at the center of the lake ($B_1 = h_1$, because $\eta = h = 0$, (1.7)).

$$\begin{aligned}
&\frac{\partial U_{12}}{\partial t} \approx g' \frac{h_1}{2L} + \frac{u_*^2}{h_1} = g' \frac{h_1}{2L}\left(1 \pm \frac{1}{W_N}\right) \\
&W_N = \left(\frac{g' h_1^2}{2 L u_*^2}\right) \\
&\partial h \approx h_1; \quad \partial x \approx L; \quad B_1 \approx h_1 \\
&g' = g\left(1 - \frac{\rho_1}{\rho_2}\right)
\end{aligned} \tag{1.7}$$

For steady-state conditions, the reduced gravity pressure gradient balances the surface wind stress and their ratio provides the Wedderburn Number (W_N, (1.7)); the factor of two is typically dropped (Thompson and Imberger, 1980; Spigel and Imberger, 1980; Monismith 1986). The Wedderburn Number approximates the steady-state balance between the reduced gravity pressure gradient and the surface wind stress when the density interface intersects the surface at the upwind end of the lake; at this point $W_N = 1$ (Monismith, 1986).

In (1.7), the plus-minus $1/W_N$ represents the direction of the wind stress relative to the baroclinic pressure gradient, which has been obfuscated by replacing the stress terms in (1.2) with W_N. If the wind stress opposes the relaxation of the tilt, then W_N is negative. If the wind stress enhances the relaxation of the tilt, then W_N is positive (Figure 1. 9).

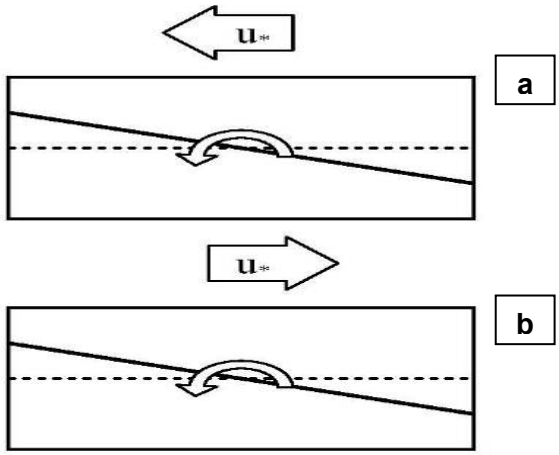

Figure 1. 9. Schematic of the two-layer model for (1.1) (a) and how wind stress enhances the relaxation of the tilt (a) and opposes the relaxation of the tilt (b). The wind stress direction is depicted by the arrow annotated with u_* and the tilt relaxation is denoted by the semi-circular arrow.

At the end of the lake, the deflection of the tilt can be approximated by W_N as (Stevens and Lawrence, 1997).

$$\zeta = \frac{kh_1}{W_N} \tag{1.8}$$

Where ζ is the interface deflection from the static position and k is a symbolic coefficient generally of order one but for the two-layer model, k=0.5 (Stevens and Lawrence, 1997). The Wedderburn Number can also be used to assess the time for the tilt to reach the equilibrium tilt. For W_N near one, the tilt reaches the equilibrium position in approximately time T/4, but for stronger wind stress the tilt reaches the surface in time approximated by (Stevens and Imberger, 1996).

$$\frac{T}{2\pi}\arccos\left(1\text{-}\mathrm{W_N}\right) \tag{1.9}$$

Where T is free seiche period (1.6). The Wedderburn Number was derived for the linear horizontal momentum equation, which is acceptable for determining the set-up of the internal wave (Stevens and Imberger, 1996; Horn, Imberger and Ivey, 2001). Stevens and Imberger (1996) suggested the non-linear terms can be ignored for Lake Numbers between 0.2 and 3.2 and small depth-to-length aspect ratios.

The Lake Number is an integral form of the Wedderburn Number (Imberger and Patterson, 1990), and it is the ratio of the baroclinic moment divided by the surface wind force moment:.

$$L_N = \frac{M_{bc}}{\tau A Z_v}$$

$$M_{bc} = mg\left(Z_G - Z_V\right)\sin\beta \qquad (1.10)$$

$$\sin\beta \approx 2Z_T / L$$

Where M_{bc} is baroclinic moment about the center of volume, A is surface area, and Z_T is the depth to the middle of the density gradient, see Figure 1. 10 for definition of other terms).

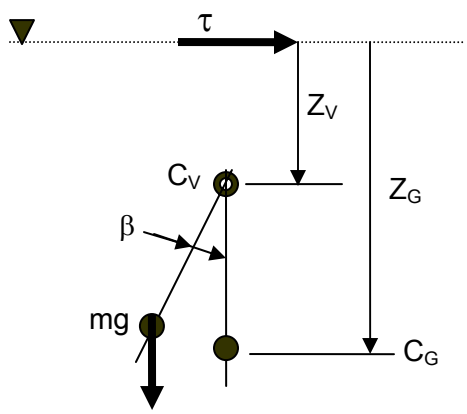

Figure 1. 10. Schematic showing how the momentum for the Lake Number is calculated. C_V is the center of volume, Z_V is the depth to C_V, C_G is the center of gravity, Z_G is the depth to C_G, mg is the body force, β is the angle of rotation of the isotherm tilt, and τ is the surface wind stress.

The Wedderburn and Lake Number have been used to assess when and by how much the isotherm tilts under a known surface wind stress and vertical density structure (Imberger and Patterson, 1990; Stevens and Lawrence, 1997). Typically, the interest was in knowing when upwelling occurred at the upwind end of the lake and assessing vertical mixing in the surface layer (Imberger and Patterson, 1990). Up to this point, only a two-layer system has been considered. Work has been done for three-layer and continuously stratified systems (Monismith, 1985, 1986, and 1987; Stevens and Imberger, 1996).

Three-layer systems can have two vertical modes of internal wave dynamics while continuously stratified systems can have an infinite number of vertical modes. The additional internal wave forms introduce additional complexity that is not captured in the two-layer model. The two-layer model allows one internal wave mode in the

vertical with the fundamental mode being a mode one vertical mode one horizontal wave (V1H1). Two-layer theory shows upwelling occurs for $W_N<1$ but upwelling can occur for $W_N>>1$ because the stratification may represent an n-layer system where n>2 (Monismith, 1986). For a three-layer system, setting the upper layer depth equal to $h_1+h_2/2$ would give a larger Wedderburn Number than setting the upper layer depth equal to h_1 (Figure 1. 11). If the internal wave response had a second mode form, then upwelling would occur for $W_N>1$ if $h_1+h_2/2$ was used for the upper layer depth instead of h_1 (Imberger and Patterson, 1990). The Wedderburn Number is subject to the selection of the appropriate upper layer depth, but the Lake Number is a more robust measure of the mode one response (Imberger and Patterson, 1990).

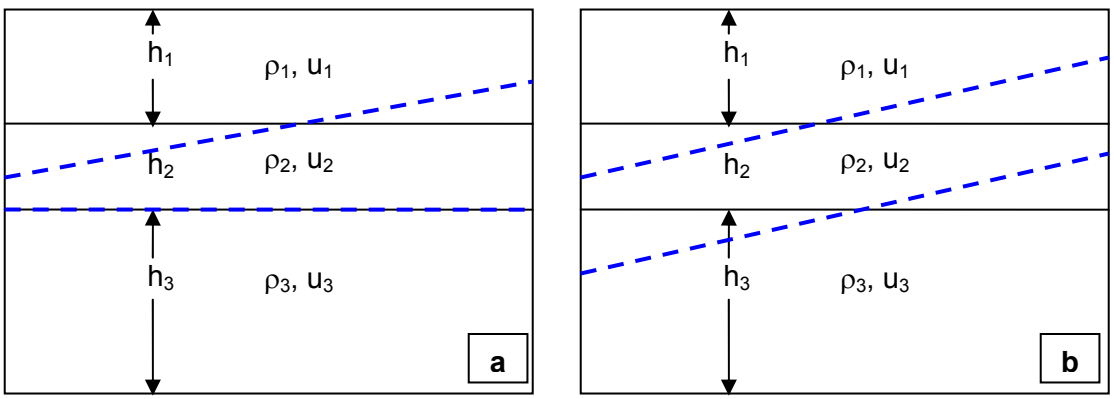

Figure 1. 11. Schematic of a simple three-layer system comprised of a surface layer (h_1), middle layer (h_2), and bottom layer (h_3). A second mode vertical and first mode horizontal response (dashed blue line) is shown in (a) and a first mode vertical and first mode horizontal response (dashed blue line) is shown in (b) (Imberger and Patterson, 1990).

occurs for small W_N and large L_N, small refers to values less than 10 (Table 1. 5). When the modal structure of the internal wave is the first mode, the deflection (1.8) and temporal (1.9) responses are appropriate.

Table 1. 5. Internal wave response for combinations of W_N and L_N. Information obtained from Stevens and Imberger (1996) and Imberger and Patterson (1990).

Parameter	$W_N<<1$	$W_N>>1$
$L_N<<1$	Large-scale tilting for $T_w>T/4$ and 1st Mode for $L_N<1$ and $W_N<1$	Deep seiching no upwelling ($L_N<1$)
$L_N>>1$	2nd Mode for long T_w, small scale deeper seiching	Small amplitude seiching
Tw is the wind duration		

For a linear stratified system, the Wedderburn Number (1.11) and internal wave period (1.12) are calculated using the buoyancy frequency (Monismith, 1986).

$$W_N = \frac{N^2 H^3}{8u_*^2 L} \tag{1.11}$$

$$T_N = \frac{2\pi L}{NH} \tag{1.12}$$

Where N is the buoyancy frequency and T_N is the approximate first mode internal wave period.

While the system may start out linearly stratified, surface mixing modifies it into a two-layer system; the upper layer is well mixed but the bottom layer is still linearly stratified. Prior to the application of the surface stress, W_N is calculated by (1.11). After the steady-state ($6T_N$) application of the surface stress, the surface layer is well mixed and the system is essentially two-layer with W_N is calculated by (1.7) (Monismith, 1986). In continuously stratified systems, there are an infinite number of layers and the density jump between each layer will be small. For the layers near the surface, their effective Wedderburn Number would be much smaller than a Wedderburn Number calculated for an equivalent two-layer system over the whole water column (the same wind stress is applied). Thus for the continuous case, the near surface layers will upwell and mix until the density jump and surface layer depth increase and reach a state similar to the two-layer case.

1.2.3.2 <u>Calculating the Wedderburn and Lake Number for Lake Washington</u>

The Wedderburn and Lake Numbers require the density differences between the two layers before application of the imposed wind stress. After the wind stress has been imposed, the baroclinic gradient is non-zero and the density interface (isotherm) tilts to balance the imposed wind stress. This tilt changes the vertical density profile along the length of the lake: warm surface water is pushed downwind, cooler bottom water is pushed upwind, and vertical entrainment occurs between the two layers (Figure 1. 12; Imberger and Patterson, 1990). If upwelling occurs, then bottom water is mixed into the surface layer at the upwind end of the lake and the vertical density profile is further modified. Thus, a continuous density time series measures the dynamic change in the Wedderburn Number that is due to the applied wind stress. A continuously stratified lake would show more vertical density structure than the discrete two-layer lake.

The thermistor arrays only spanned part of the water depth so only part of the vertical density profile was known for calculating W_N and L_N (Table 1. 2), and for year 2003 there was no centrally located thermistor array. To compensate for these limitations and to account for the dynamic effects between wind and tilt, the layer density difference for W_N was estimated using the averaged density of the lower two thermistors of the southernmost site less the average density of the upper two thermistors of the northernmost site (Figure 1. 12). This method was used for the 2003 and 2004 data to be consistent, and because the 2004 MWY array profiles sometimes showed the vertical density gradient as zero when the lake was stratified. This condition occurred during large tilts, which dropped below the thermistor array leaving the array entirely within the upper surface layer.

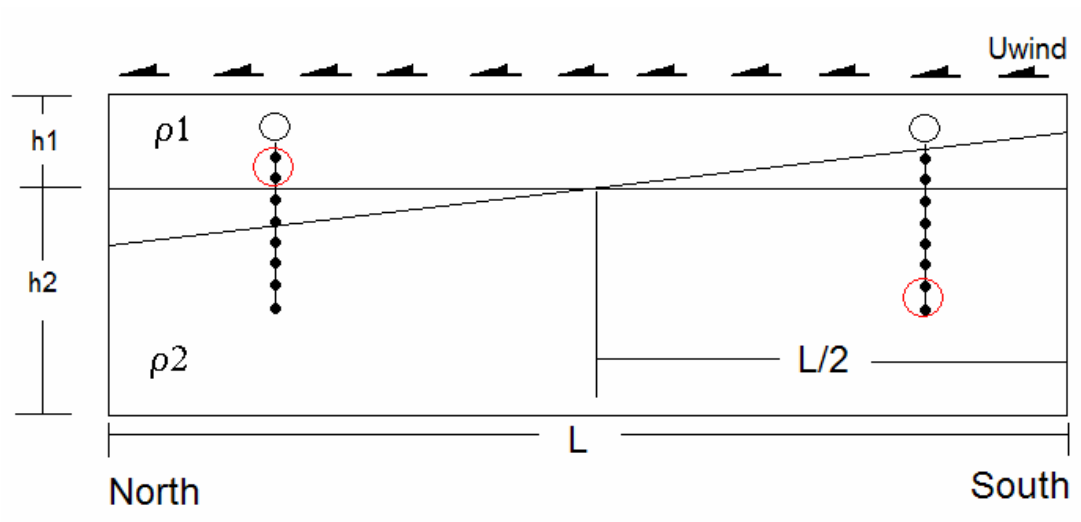

Figure 1. 12. Density interface tilt that results from a wind stress applied at the water surface. The horizontal line is the static position before the wind stress and the tilted line is the resultant tilt from the applied wind stress. Two thermistor arrays are shown to the north and south of the center of rotation. The two upper and lower thermistors were selected (circles) to estimate the density difference over the depth.

RBR and SCAMP temperature profiles indicate the northern upper two thermistors approximate the average temperature, but the southern lower two thermistors may estimate cooler temperatures during some events (Figure 1. 13 and Figure 1. 14). For April 10, 2003, the $SR520_C$ upper two RBR thermistor temperatures lie between the MWY and NOA SCAMP temperatures above the 30-meter depth that represents the upper layer (Figure 1. 13). The SWA lower two RBR thermistor temperatures are

less than the SWA SCAMP temperature, but they do lie below the temperature step at about 22 meters. For the 2004 data, the NOA upper two RBR thermistor temperatures are typically warmer than the SCAMP data (possibly an instrumentation difference), but they represent the upper layer temperature (Figure 1. 14). The SWA lower two RBR thermistor temperatures represent to coolest water on March 9, but are representative of bottom temperatures for March 30 and April 16, 2004. Using the northern upper two RBR thermistors and southern bottom two RBR thermistors reasonably approximates the density difference for calculating the Wedderburn Number. At times, the approximation may overestimate the density difference, giving a slightly larger Wedderburn Number.

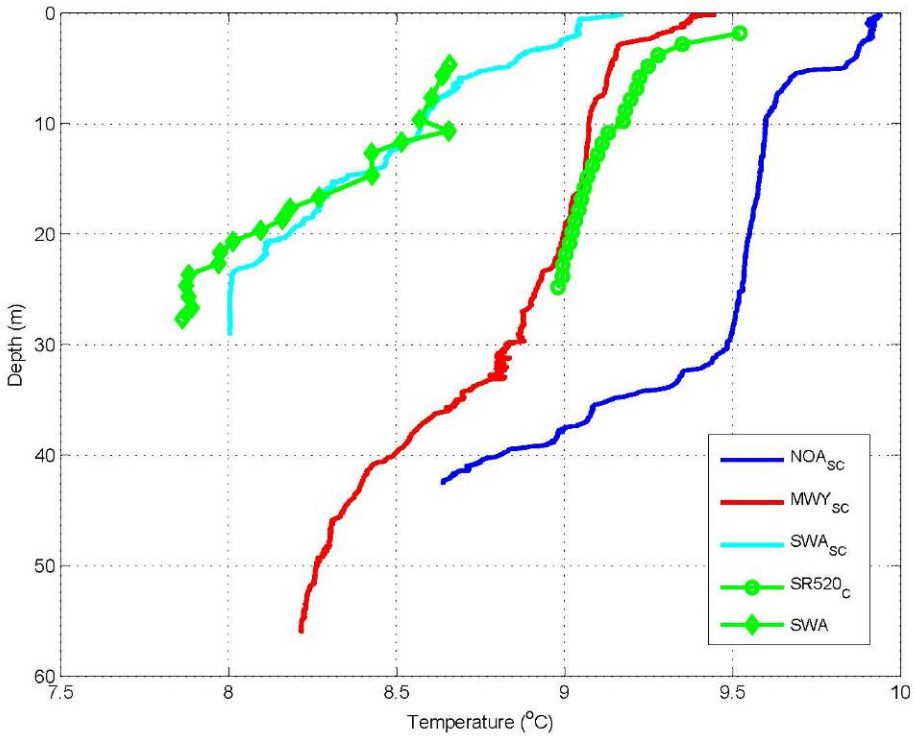

Figure 1. 13. Temperature profiles from the SCAMP and RBR on April 10, 2003. SCAMP profiles were taken at NOA (blue), MWY (red), and SWA (cyan) and the RBR profiles were taken at SR520$_C$ (circles) and SWA (diamonds); thermistors are demarcated by the circles or diamonds.

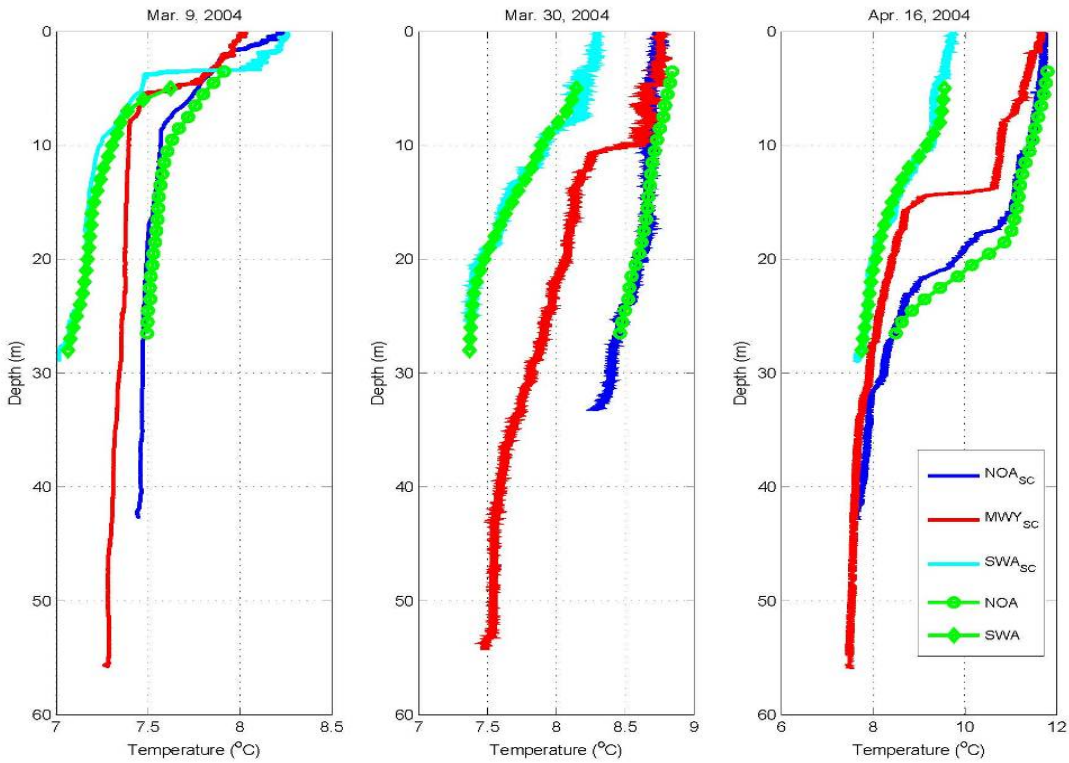

Figure 1. 14. Temperature profiles from the SCAMP and RBR on March 9, March 30, and April 16 of 2004. SCAMP profiles were taken at NOA (blue), MWY (red), and SWA (cyan) and the RBR profiles were taken at NOA (circles) and SWA (diamonds); thermistors are demarcated by the circles or diamonds.

When calculating the Wedderburn Number, the friction velocity should be low-pass filtered with a filter length equal to one-quarter of the period of the first mode internal wave (T/4); a saw-tooth filter was used (Stevens and Imberger, 1996; Stevens and Lawerence, 1997). The filter smoothes the high frequency response of the wind field relative to the low frequency response of the internal wave. The saw-tooth form decreases the influences of previous wind events. The upper layer depth was estimated from SCAMP temperature and fluorescence profiles, which identifies the vertical distribution of chlorophyll *a* or phytoplankton. Specific values for the filter length and layer depths are given in the Results section.

The Lake Number was calculated using the RBR thermistor profiles and bathymetry-area information was obtained from data files used in a hydrodynamic model for Lake Washington (Johnson, Kim, and Nail, 2003). SR520C and SR520N1 data were combined for calculating L_N for 2003 and the MWY data was used for 2004;

SR520N1 thermistors from 26 to 40 meters were added to the SR520C observations. The friction velocity was filtered with the same saw-tooth filter design used for the Wedderburn Number.

1.2.3.3 Temporal and Spatial Representation of the Isotherms

The Wedderburn and Lake Numbers provide a scalar quantity that can be used to assess how important wind stress is in determining the dynamics of the isotherms (internal waves). However, to verify the relation between W_N, L_N, and the isotherms one must compare the scalar series against the isotherm series. The structure of the isotherms can be very complicated and difficult to interpret as a whole. For this reason, various methods have been developed to reduce the isotherm structure into fewer salient features.

These methods typically integrate a selected set of isotherms into a single time series or select a few isotherms that represent the system (Stevens et al, 1996; Wiegand and Chamberlain, 1987; Antenucci, Imberger, and Saggio, 2000; Munnich, Wuest, Imboden, 1992; Roget, Salvade, and Zamboni, 1997). The integrated method retains first vertical modes but depresses higher order vertical modes (Antenucci, Imberger, and Saggio, 2000). Retaining an isotherm set keeps the higher modal features but requires selecting the appropriate isotherms that contain the desired modal features (Roget, Salvade, and Zamboni, 1997). For the temperature array data obtained, selection of a single isotherm was not possible over the observed time series, let alone several; therefore, a more robust method was needed. Principal Component Analysis was selected to analyze the temperature array data.

Principal Component Analysis (PCA) is an eigenvalue problem that transforms N correlated time series observations into N uncorrelated time series observations but comprised of two functional forms: an eigenvector (EV) set that describes a physical shape and an expansion coefficient (expansion coefficients) set that describes the temporal evolution of each eigenvector (Haan, 1977; Bjornsson and Venegas, 1997). PCA decomposes the variance of a set of N observations into N orthogonal observations; usually, the first orthogonal series describes the greatest amount of variance (contains the most information about the observations), the second

orthogonal series describes the next greatest amount of variance and each subsequent orthogonal series contains less variance. PCA methods have the advantage of decomposing the N time series observations into a few orthogonal time series that contain most of the pertinent information (Haan, 1977). PCA methods have been used to analyze single-scalar field variables for a variety of geophysical observations such as sea surface temperature and pressure, hydraulic flow regimes, and estuary flow patterns, to name a few (Bjornsson and Venegas, 1997; Mountain and Taylor, 1998; Liu, Zarillo, and Surak, 1997; Koutitonsky, Wilson, and El-Sabh, 1990: McPhanden and Hayes, 1991). In this study, PCA analysis will be used to decompose temperature array series into a few dominant modes.

PCAs do not provide context for the shape of the eigenvectors or the expansion coefficients; this is left to the insight of the user. Because the user must determine the relation between the PCA results and observations, a brief presentation follows of how the PCA results describe the temperature observations. The modal velocity structure is described by superposition of a set of eigensolutions (Gill, 1982).

PCA partitions the total variance into a set of orthogonal functions that are determined by the observed data. This study is interested in the vertical variation of density, which is represented by the isotherms. The vertical isotherm displacement is determined by the vertical velocity, which is defined by the modal form of the internal wave. At the density interface, the vertical velocity (w) is the total derivative of the interfacial displacement (h) (1.13), which can be approximated by the linear form given by (1.14)

$$w = \frac{dh}{dt} = \frac{\partial h}{\partial t} + u\frac{\partial h}{\partial x} + w\frac{\partial h}{\partial z} \tag{1.13}$$

$$w = \frac{\partial h}{\partial t} \tag{1.14}$$

Assuming a sine form for the vertical velocity (Gill, 1982), the vertical displacement of the density interface has a cosine form (1.15).

$$\begin{aligned} w &= w_0 \sin(\omega t) \\ h &= \frac{w_0}{\omega}\cos(\omega t) \end{aligned} \tag{1.15}$$

Where w_0 is the velocity amplitude, ω is frequency and w_0/ω is the amplitude of the interface displacement. Assuming the density will as a step structure given by (1.16)

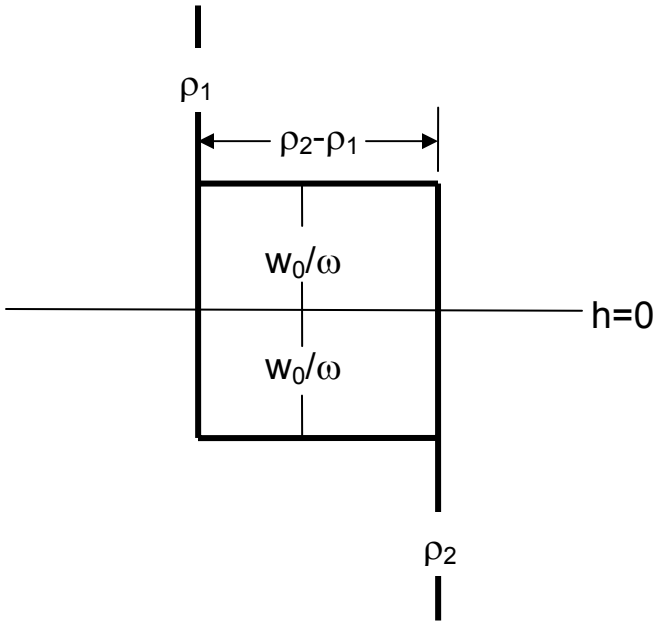

Figure 1. 15. Vertical excursion of the two-layer density interface that is subject to an oscillation with amplitude w_0/ω. The upper layer density is $\rho 1$ and the lower layer density is $\rho 2$. Within the excursion, the maximum density difference is $\rho 2$-$\rho 1$. The static position is at h=0.

$$\begin{aligned} \rho &= \rho_1, \quad z > h \\ \rho &= \rho_2, \quad z < h \end{aligned} \tag{1.16}$$

Where z is the water depth above or below the interface displacement h.

The density interface will oscillate over a depth of $2w_0/\omega$ over the period T when isotherm displacement is governed by internal waves. Within the excursion, the density difference will be ρ_2-ρ_1 but outside the excursion the density difference will be zero (Figure 1. 15); the density variance is zero above and below the steps and it is greater than zero within the excursion. When isotherm displacement is caused by internal wave dynamics, the modal shape of the vertical density structure infers the modal shape of the vertical velocity. The corresponding density expansion coefficients will have the same temporal pattern as the horizontal mode of the freely oscillating internal wave. However, the vertical density structure could be controlled by the heat flux across the water surface.

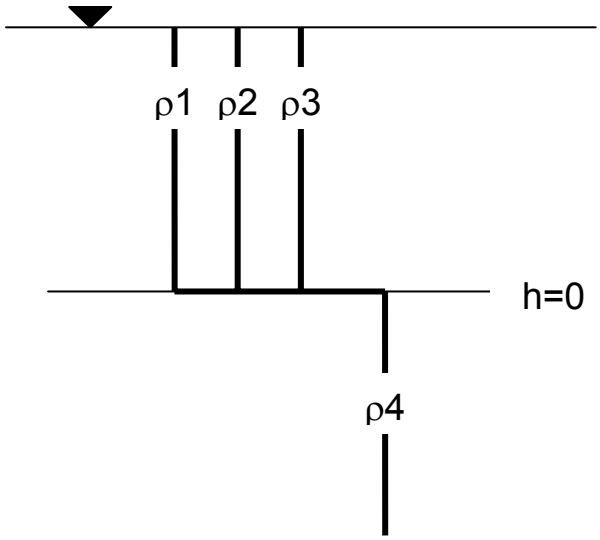

Figure 1. 16. Density variations caused by surface heat flux at the water surface. Internal wave oscillations at the density interface are negligible. Surface density ranges from $\rho 1<\rho 2<\rho 3$ but the bottom density ($\rho 4$)is relatively unaffected.

Surface heat flux across the water surface will affect density in the upper layer (Figure 1. 16) and the expansion coefficients will have a temporal pattern associated with the net surface layer heat balance (McPhaden and Hayes, 1991). In this case, the density interface remains stationary unless vertical entrainment at the interface occurs. Above the interface the density variance is greater than zero, while below the interface density variance is zero. Generally, internal wave dynamics will produce a sub-surface variance maximum similar to the modal vertical velocity, while surface heat flux will produce a monotonically decreasing variance. The corresponding expansion coefficients will be correlated with the process driving the density variance.

1.3 Results

The Wedderburn, Lake Number, and temperature PCA are calculated in this section. The three series are qualitatively compared to present causal relations between surface wind stress and isotherm tilting. Because PCA does not provide context to the eigenvectors and expansion coefficients, the physical meaning of the PCAs are determined first, then the W_N and L_N are compared to the PCAs. Before the temperature and velocity data were decomposed, temporal trends were removed by curve fitting. Once the data was de-trended, the data was organized with time measures in rows and spatial measures in columns; this form is termed an S-mode analysis (Bjornsson and Venegas, 1997). The PCAs were compared to the

observed temperature data to assess the internal seiche structure that determines the vertical and horizontal temperature distribution (isotherms) in Lake Washington. SCAMP temperature and fluorescence profiles are also reviewed to assess isotherm tilts at specific times of the study period.

1.3.1 PCA Decomposition of Temperature and Velocity Profiles

1.3.1.1 April 2003 Observations

The SR520N1 and SR520C arrays were located about 200 meters apart with the SR520N1 array covering the water column from 16 – 40 meters and the SR520C covering the water column from 2 – 25 meters (Table 1. 2). Because the arrays were so close, SR520N1 data from 26 – 40 meters was appended to the SR520C data, effectively increasing the covered water column from 2 – 40 meters. The combined data set is hereafter referred to as SR520.

For the SR520 and SWA temperature array data, data were interpolated to a common depth interval and the average density was determined (Figure 1. 17a). At SR520, the average density time series was less than the average density at SWA up to about JD 112 after which the mean densities oscillated about each other. Each density time series was de-trended using a fitted curve and density perturbations were determined by subtracting the fitted curve from the average density (Figure 1. 17b). The SWA density perturbations are 180° out of phase with the SR520 density perturbations. This response is consistent for a horizontal internal seiche for an odd-numbered mode (first mode, third mode, fifth mode, etc.).

Eigenvectors for temperature and north-south velocity are presented in Figure 1. 18 and percent of total variance is given in Table 1. 6. Expansion coefficients are given in Figure 1. 19 for the first and second modes. Eigenvectors represent the physical structure and the expansion coefficients represent the temporal evolution of the eigenvector; the convolution of the two recreates the variable in space and time. For example, the first mode eigenvector for velocity is positive for depths less than about 22 meters and is negative for depths greater than 22 meters (Figure 1. 18c). A positive expansion coefficient means velocity is positive above 22 meters and negative below 22 meters. A negative expansion coefficient means velocity is negative above 22 meters and positive below 22 meters. The first mode velocity will

oscillate about 22 meters where the velocity is always zero because the eigenvector is always zero (Figure 1. 20).

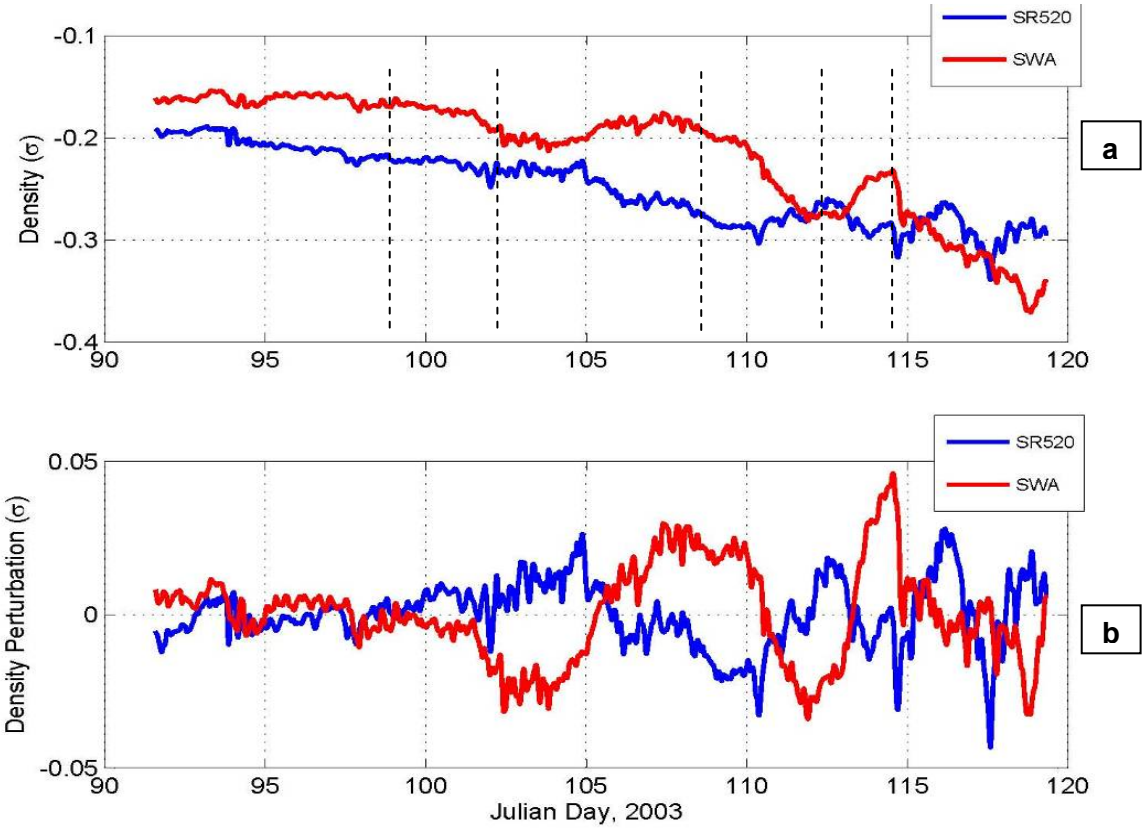

Figure 1. 17. April 2003 time series of the averaged density (a) ($\sigma=\rho-1000$ (kg/m^3)) at SR520 and SWA and the corresponding density perturbation (observed less trend) (b). Temperature readings were interpolated to a common depth interval between the two locations. Vertical dashed lines represent periods defined in section 1.3.3.1.

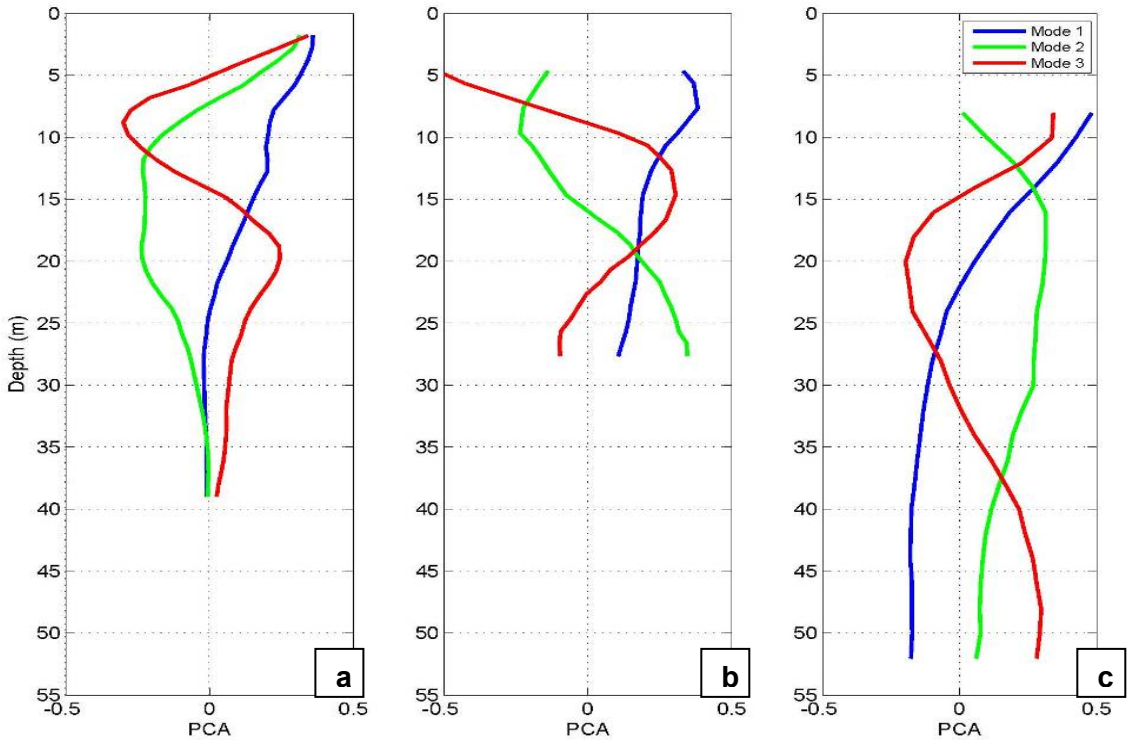

Figure 1. 18. April 2003 eigenvector modes for temperature and the north-south velocity component (VN) at SR520 (a), SWA (b), and MWY (c). Percent of variance for the dominant modes is given in Table 1. 6.

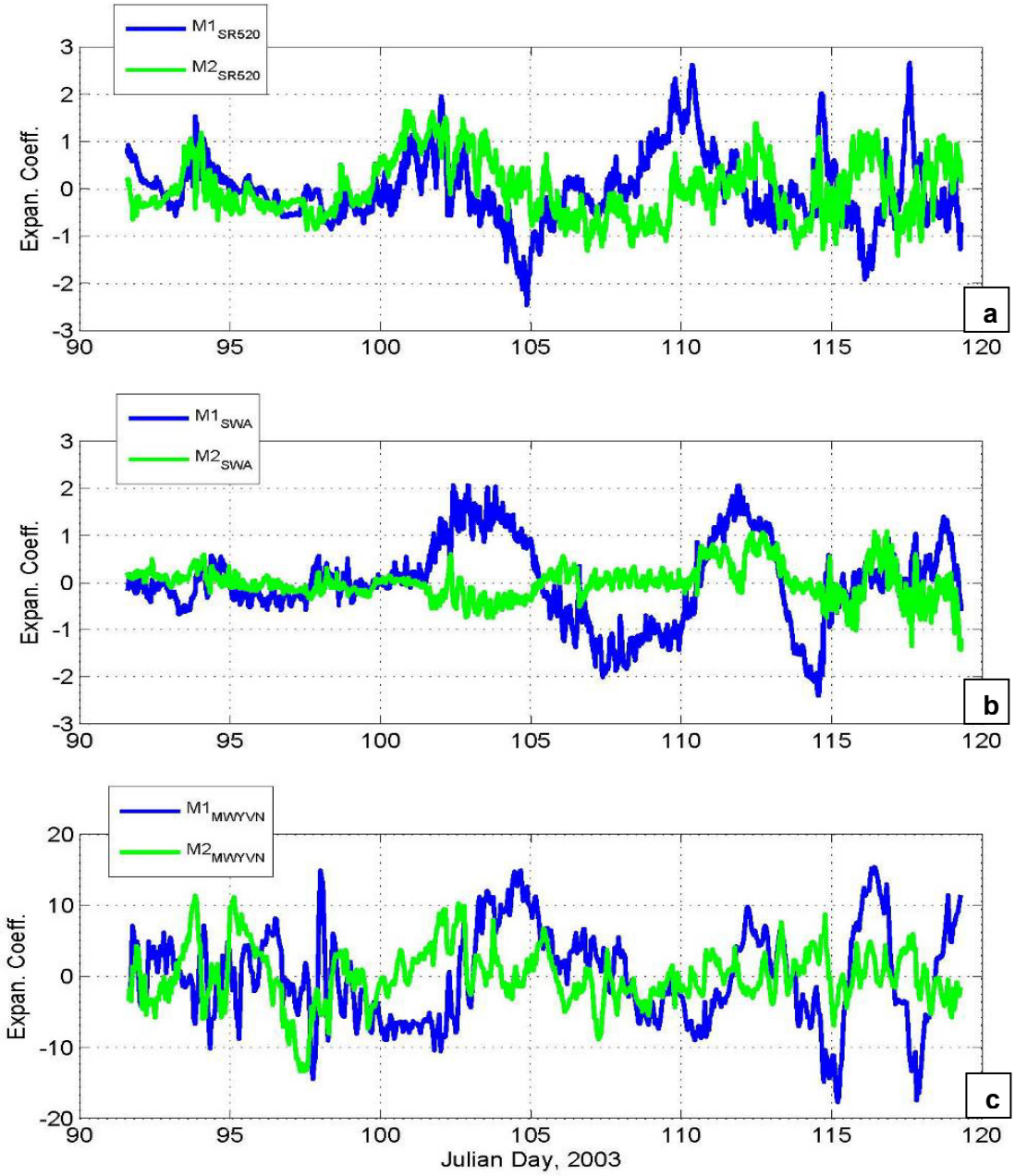

Figure 1. 19. April 2003 expansion coefficients for the mode one (blue) and mode two (green) eigenvectors presented in Figure 1. 18. SR520 is (a), SWA is (b), and MWY is (c).

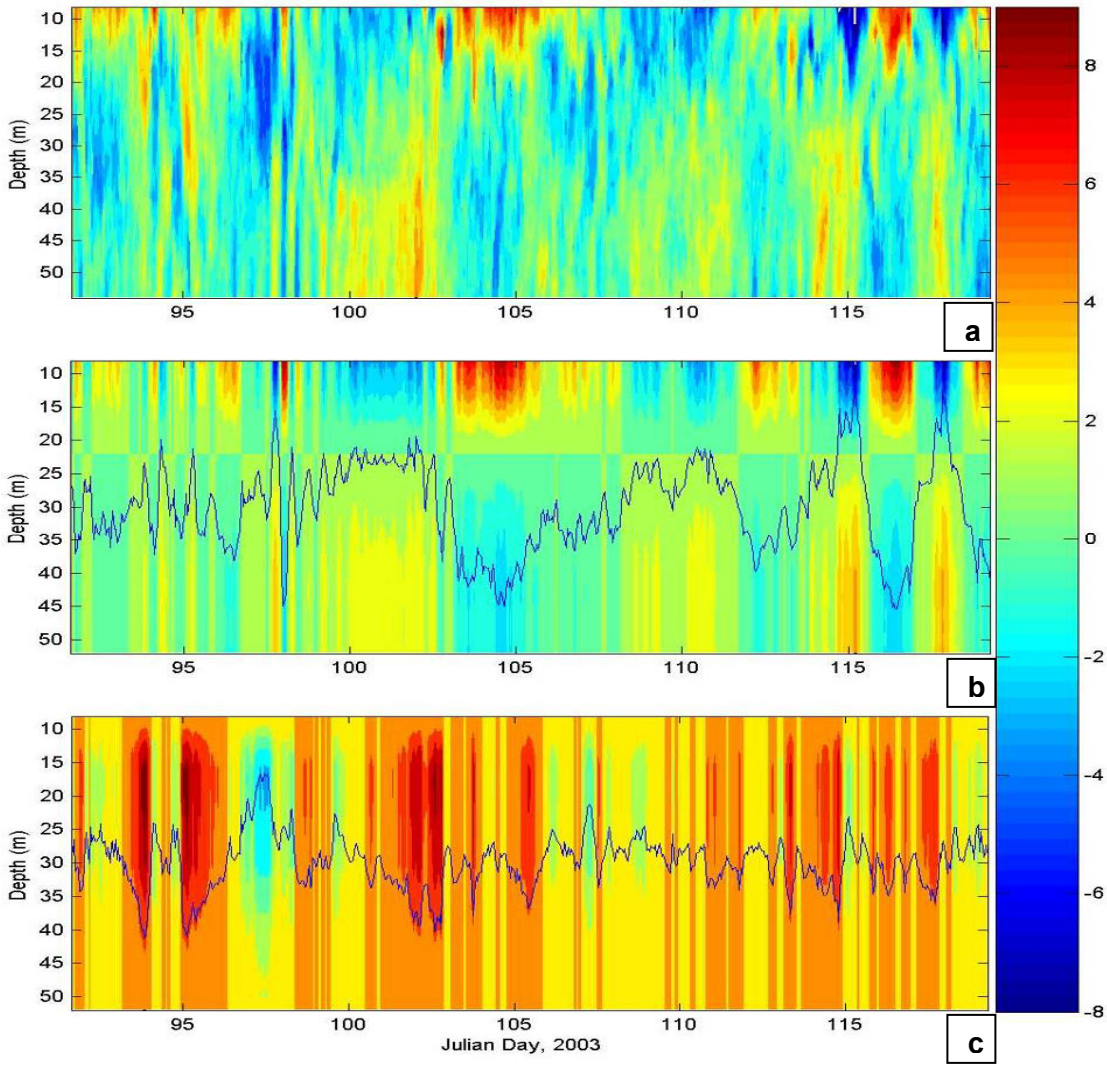

Figure 1. 20. Observed north-south velocities at MWY (a) and the decomposed PCA mode one (b) and mode two (c) north-south velocities. The mode one and two expansion coefficients are superimposed on the contour plots and centered at the 30-meter depth. Color contours have units of (cm/s) with positive being north.